Static SPME sampling of VOCs emitted from indoor building materials: prediction of calibration curves of single compounds for two different emission cells

Pierre Mocho, Valérie Desauziers

▶ **To cite this version:**

Pierre Mocho, Valérie Desauziers. Static SPME sampling of VOCs emitted from indoor building materials: prediction of calibration curves of single compounds for two different emission cells. Analytical and Bioanalytical Chemistry, 2011, 400 (3), pp.859-870. 10.1007/s00216-011-4820-y . hal-04183033

HAL Id: hal-04183033

https://imt-mines-ales.hal.science/hal-04183033

Submitted on 2 Nov 2023

HAL is a multi-disciplinary open access archive for the deposit and dissemination of scientific research documents, whether they are published or not. The documents may come from teaching and research institutions in France or abroad, or from public or private research centers.

L'archive ouverte pluridisciplinaire **HAL**, est destinée au dépôt et à la diffusion de documents scientifiques de niveau recherche, publiés ou non, émanant des établissements d'enseignement et de recherche français ou étrangers, des laboratoires publics ou privés.

Static SPME sampling of VOCs emitted from indoor building materials: prediction of calibration curves of single compounds for two different emission cells

Pierre Mocho · Valérie Desauziers

Abstract Solid-phase microextraction (SPME) is a powerful technique, easy to implement for on-site static sampling of indoor VOCs emitted by building materials. However, a major constraint lies in the establishment of calibration curves which requires complex generation of standard atmospheres. Thus, the purpose of this paper is to propose a model to predict adsorption kinetics (i.e., calibration curves) of four model VOCs. The model is based on Fick's laws for the gas phase and on the equilibrium or the solid diffusion model for the adsorptive phase. Two samplers (the FLEC® and a home-made cylindrical emission cell), coupled to SPME for static sampling of material emissions, were studied. A good agreement between modeling and experimental data is observed and results show the influence of sampling rate on mass transfer mode in function of sample volume. The equilibrium model is adapted to quite large volume sampler (cylindrical cell) while the solid diffusion model is dedicated to small volume sampler (FLEC®). The limiting steps of mass transfer are the diffusion in gas phase for the cylindrical cell and the pore surface diffusion for the FLEC®. In the future, this modeling approach could be a useful tool for time-saving development of SPME to study building material emission in static mode sampling.

P. Mocho
Laboratoire Thermique Energétique et Procédés—Université de Pau et des Pays de l'Adour, BP,
7511–64075 Pau, France

V. Desauziers (✉)
Laboratoire Génie de l'Environnement Industriel—Ecole des Mines d'Alès, Hélioparc, 2 Avenue Pierre Angot,
64053 Pau Cedex 9, France
e-mail: valerie.desauziers@mines-ales.fr

Keywords Volatile organic compounds · Indoor air · Material · Emission · Solid-phase microextraction · Adsorption modeling · Calibration curves prediction

Introduction

Volatile organic compounds (VOCs) are of environmental interest because they can be responsible for health hazards and/or malodorous atmospheres [1, 2]. With regard to the number of sources in building environments, they are found to be present at higher concentrations in indoor air than in outdoor air [3]. To limit their levels, one strategy relies on the control of their major emission sources, especially building materials [4, 5]. In France as in several European countries, new products are evaluated through a time-consuming procedure involving a 28-day emission test in an environmental chamber or in an emission cell [6]. The protocol is based on a dynamic sampling mode to transfer the VOCs emitted from the material to an adsorbent tube to concentrate the compounds. Thus, clean air supply, air flow meters, controlled temperature and hygrometry are needed. These protocols, covered by ISO standards [7, 8], are adapted to laboratory testing for material labeling but are not able to evaluate the material behavior in field in the aim of determining their impact in indoor air quality. For this purpose, static sampling methods [9–11] are recently investigated for simpler and faster on-site sampling. One of these methods is developed in our laboratory [12, 13]. It consists of coupling a standard FLEC® emission cell with solid-phase microextraction (SPME) for rapid sampling and simple thermal desorption, directly performed in GC injector. FLEC®-SPME sampling involves two steps: first, VOCs diffusion from the material to the gas phase (FLEC® headspace) and second, after introduction of SPME in the

FLEC®, the VOCs transfer from the gas phase to the fiber. Assuming equilibrium is reached in the FLEC®, the headspace concentration could be assimilated to the gas phase concentration at the material surface. A PDMS-Carboxen fiber is chosen owing to its performance assessed in previous studies [14]. However, because of the thickness of the adsorbent coating layer, competitive adsorption leading to inaccurate quantification can be observed [15, 16]. To overcome this drawback, operating conditions should be carefully determined in terms of sample volume and extraction time [16–24]. Another constraint of the SPME technique lies in the establishment of calibration curves which needs complex generation of standard gas atmospheres. Thus, the purpose of this paper is first to propose a predictive model of calibration curves based on Fick's law and Langmuir isotherm, to simplify the calibration protocol. A second model named solid diffusion model is also developed to take into account, if necessary, both the diffusion in gas and solid phases. The second objective is to study the mechanism of mass transfer in two emission samplers of different volumes and geometries: the FLEC®, we firstly applied to the static sampling of VOCs emissions, and a home-made cylindrical sampler. This latter is especially designed as alternative to the FLEC® to improve sensitivity by increasing the volume and to reduce the cost in case of multipoint sampling in the field. The developed models are tested by comparing the experimental and theoretical adsorption kinetics of 4 single VOCs often found in building material emissions and presenting different affinities for the Carboxen SPME fiber [12].

Theoretical basis

Adsorption kinetics modeling is based on Fick's laws for the gas phase and on the equilibrium or the solid diffusion model for the adsorptive phase. A control-volume method is implemented to develop the model.

Gas phase mass transfer

Development of the equation starts from consideration of an element of tube located in radial and axial coordinates r,z of radial thickness Δr and axial height Δz, as shown in Fig. 1, according to the geometry of the gas samplers described in the Experimental section. Radial and axial diffusive flows (F_{ri}, F_{ro}, F_{ai}, F_{ao}) enter and leave the element and are described hereafter:

$$F_{ri} = D_G\left(2\pi\left(r+\frac{\Delta r}{2}\right)\Delta z\right)\left(\frac{dC}{dr}\right)_{r+\Delta/2,z} \quad (1)$$

$$F_{ro} = D_G\left(2\pi\left(r-\frac{\Delta r}{2}\right)\Delta z\right)\left(\frac{dC}{dr}\right)_{r-\Delta r/2,z} \quad (2)$$

$$F_{ai} = D_G(2\pi r\Delta r)\left(\frac{dC}{dz}\right)_{r,z-\Delta z/2} \quad (3)$$

$$F_{ao} = D_G(2\pi r\Delta r)\frac{dC}{dz}_{r,z+\Delta z/2} \quad (4)$$

Mass balance leads to the following equations:

$$F_{ri} + F_{ai} - F_{ro} - F_{ao} = V_{r,z}\left(\frac{dC}{dt}\right)_{r,z} \quad (5)$$

$$\frac{D_G}{r}\frac{d}{dr}\left(r\frac{dC}{dr}\right)_{r,z} + D_G\left(\frac{d^2C}{dz^2}\right)_{r,z} = \frac{dC}{dt_{r,z}} \quad (5bis)$$

with C the gas concentration of the compound in the element, D_G the molecular diffusion coefficient in gas phase. The coefficient D_G is estimated by the Fuller equation [25].

Boundary conditions of Eq. (5bis) are expressed by:

$$\left(\frac{dC}{dz}\right)_{r,z} = 0 \quad (6)$$

in $r(z)=R_z$ for FLEC® and $r=R$ for cylindrical sampler

$$\left(\frac{dC}{dz}\right)_{r,z} = 0 \quad (7)$$

in $z(r)=Z_r$ for FLEC® and $z=Z$ for cylindrical sampler

The geometric data of the two samplers required to study the boundary conditions are detailed in "Experimental" section.

Adsorptive phase mass transfer

Equilibrium model

The amount adsorbed q_z on the fiber in axial coordinate z is considered in equilibrium with the gas boundary layer concentration $C_{1,z}$ in $r=r_f+\Delta r/2$ by the Langmuir model [26]:

$$q_z = \frac{Kq_mC_{1,z}}{1+KC_{1,z}}\frac{\Delta z}{h_f} \quad (8)$$

with r_f, h_f, the radius and height of the fiber, q_m the maximum amount of component adsorbed, K the Langmuir constant.

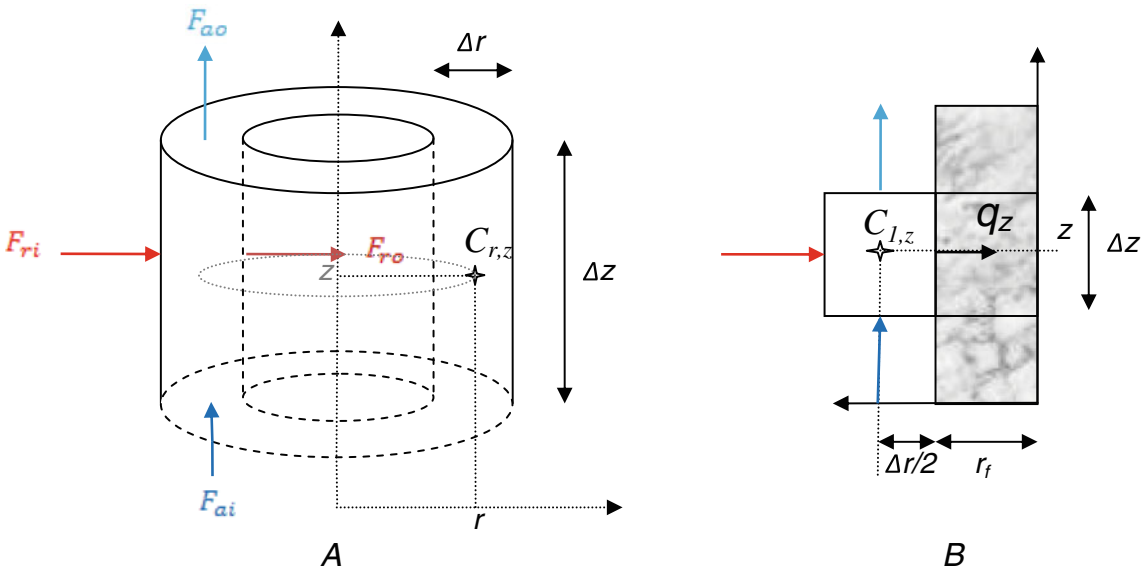

Fig. 1 Mass balance in an element of tube in gaseous phase (**a**) and in contact with adsorptive phase (**b**)

Differentiating Eq. 8 with time, one obtains:

$$\left(\frac{\mathrm{d}q}{\mathrm{d}t}\right)_{rf,z} = \frac{\mathrm{d}q_z}{\mathrm{d}C_{1,z}}\frac{\mathrm{d}C_{1,z}}{\mathrm{d}t} = \frac{\Delta z}{h_f}\frac{Kq_m}{(1+KC_{1,z})^2}\frac{\mathrm{d}C_{1,z}}{\mathrm{d}t} \text{ with } \quad C_{1,z} = C_{rf+\Delta r/2,z} \tag{9}$$

Gas phase mass balance in an element of tube in contact with the adsorptive coating yields to the following boundary condition with the gas boundary concentration $C_{1,z}$ located in $r=r_f+\Delta r/2$ (Fig. 1):

$$F_{\mathrm{ri}} + F_{\mathrm{ai}} - \left(\frac{\mathrm{d}q}{\mathrm{d}t}\right)_{rf,z} - F_{\mathrm{ao}} = V_{r,z}\left(\frac{\mathrm{d}C_{1,z}}{\mathrm{d}t}\right)_{rf+\Delta r/2,z} \tag{10}$$

$$D_{\mathrm{G}}\frac{r+^{\Delta r}/_{z}}{\Delta r}\left(\frac{\mathrm{d}C}{\mathrm{d}r}\right)_{rf+\Delta r,z} + D_{\mathrm{G}}r\left(\frac{\mathrm{d}^2C_{1,z}}{\mathrm{d}z^2}\right)_{rf+\Delta r/2,z} - \frac{1}{2\pi\Delta r\Delta z}\left(\frac{\mathrm{d}q}{\mathrm{d}t}\right)_{rf,z} = r\left(\frac{\mathrm{d}C_{1,z}}{\mathrm{d}t}\right)_{rf+\Delta r/2,z} \tag{10bis}$$

Solid diffusion model

The adsorptive coating phase is considered as a homogeneous media without distinction between the porous, the solid phases, and the nature of the material (PDMS, Carboxen) for a simplified model. Following the same methodology than previously described, mass balance, taking account only radial diffusive flow in an element of tube of radial thickness Δr_{s} and axial height Δz, leads to the following equation in the adsorptive phase (Fig. 2):

$$\frac{D_{\mathrm{s}}}{r_{\mathrm{s}}}\frac{\mathrm{d}}{\mathrm{d}r_{\mathrm{s}}}\left(r_{\mathrm{s}}\frac{\mathrm{d}q}{\mathrm{d}r_{\mathrm{s}}}\right)_{r_{\mathrm{s}},z} = \frac{\mathrm{d}q}{\mathrm{d}t_{r_{\mathrm{s}},z}} \tag{11}$$

with $q_{rs,z}$ the amount adsorbed in the element, D_{S} the solid diffusion coefficient of the compound.

Solid-phase mass balance in an external element of tube ($r_s=r_f-\Delta r_s/2$) in contact with the gas phase is expressed by:

$$D_{\mathrm{s}}\left[r_f\left(\frac{\mathrm{d}q}{\mathrm{d}r_s}\right)_{rf} - (r_f-\Delta r_s)\left(\frac{\mathrm{d}q}{\mathrm{d}r_s}\right)_{rf-\Delta r_s,z}\right] = \Delta r_s\frac{\mathrm{d}q_{nr,z}}{\mathrm{d}t}_{rf-\Delta r_s/2,z} \tag{12}$$

where nr is the number of concentric tube located on the external layer of the adsorbent.

At the solid/gas interface ($r=r_f$), flux continuity is expressed by:

$$D_{\mathrm{G}}\left(\frac{\mathrm{d}C}{\mathrm{d}r}\right)_{rf,z} = D_{\mathrm{s}}\left(\frac{\mathrm{d}q}{\mathrm{d}r_{\mathrm{s}}}\right)_{rf,z} \tag{13}$$

and the equilibrium state is assumed between $q_{\mathrm{int},z}$, the interface amount adsorbed, and $C_{\mathrm{int},z}$ the concentration at the gas interface (Fig. 2).

Gas phase mass balance in an element of tube in contact with the adsorptive coating gives the following equation located in $r=r_f+\Delta r/2$:

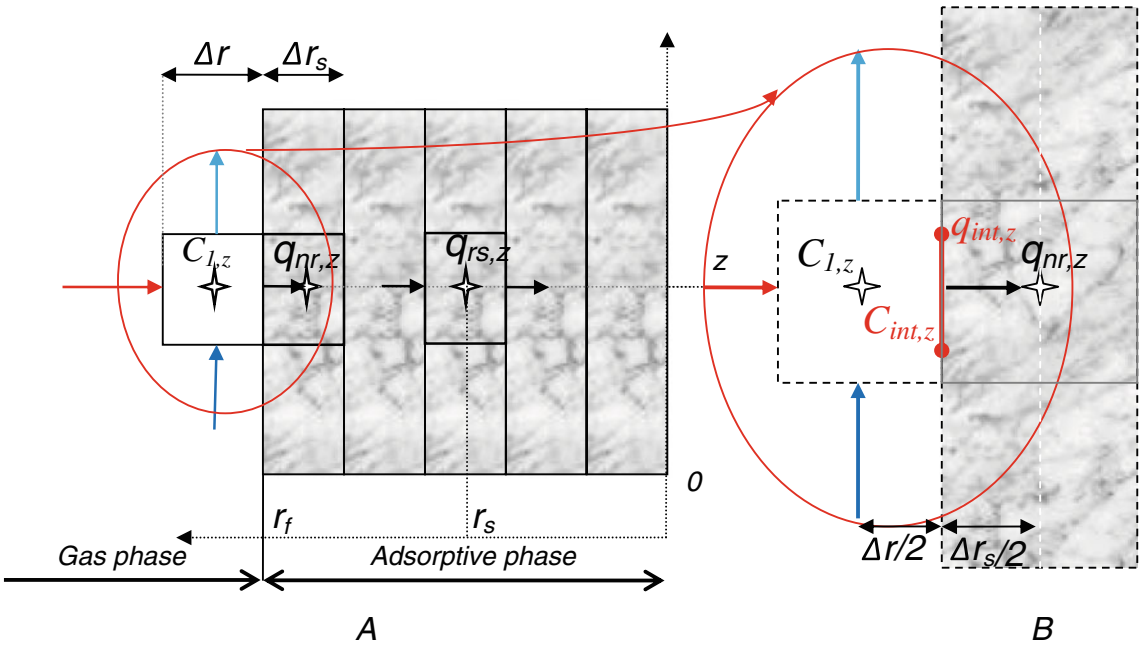

Fig. 2 Mass flux in the solid diffusion (**a**) model with interface conditions (**b**)

$$D_{\mathrm{G}}\frac{r+^{\Delta r}/2}{\Delta r}\left(\frac{\mathrm{d}C}{\mathrm{d}r}\right)_{r_{\mathrm{f}}+\Delta r,z}+D_{\mathrm{G}}r\left(\frac{\mathrm{d}^2C_{1,z}}{\mathrm{d}z^2}\right)_{r_f+\Delta r/2,z}-\frac{D_{\mathrm{s}}r_{\mathrm{f}}}{\Delta r}\left(\frac{\mathrm{d}q_{\mathrm{int},z}}{\mathrm{d}t}\right)_{r_f,z}=r\left(\frac{\mathrm{d}C_{1,z}}{\mathrm{d}t}\right)_{r_f+\Delta r/2,z} \quad (14)$$

$$\left(\frac{\mathrm{d}q_{\mathrm{int},z}}{\mathrm{d}t}\right)_{r_f,z}=\frac{\Delta z}{h_f}\frac{Kq_m}{\left(1+KC_{\mathrm{int},z}\right)^2}\left(\frac{\mathrm{d}C_{\mathrm{int},z}}{\mathrm{d}t}\right)_{r_f,z} \quad (15)$$

$$\left(\frac{\mathrm{d}C}{\mathrm{d}r}\right)r_{f,z}=\frac{2\left(C_{1,z}-C_{\mathrm{int},z}\right)}{\Delta r}\quad\text{and}\quad\left(\frac{\mathrm{d}q}{\mathrm{d}r_s}\right)r_{f,z}=\frac{2\left(q_{\mathrm{int},z}-q_{nr,z}\right)}{\Delta r_s} \quad (16)$$

By subsisting Eq. 16 in Eq. 13, we deduce:

$$C_{\mathrm{int},z}=C_{1,z}-\frac{D_{\mathrm{S}}}{D_{\mathrm{G}}}\frac{\Delta r}{\Delta r_{\mathrm{s}}}\left(q_{\mathrm{int},z}-q_{nr,z}\right) \quad (17)$$

Differentiating Eq. 17 with time, we obtain:

$$\left(\frac{\mathrm{d}C_{\mathrm{int}}}{\mathrm{d}t}\right)_{r_f,z}=\left(\frac{\mathrm{d}C_{1,z}}{\mathrm{d}t}\right)_{r_f+\Delta r/2,z}-\frac{D_{\mathrm{S}}}{D_{\mathrm{G}}}\frac{\Delta r}{\Delta r_s}\left(\left(\frac{\mathrm{d}q_{\mathrm{int},z}}{\mathrm{d}t}\right)_{r_f,z}-\left(\frac{\mathrm{d}q_{nr,z}}{\mathrm{d}t}\right)_{r_f-\Delta r_s/2,z}\right) \quad (18)$$

By substituting Eq. 15 in Eq. 18,

$$\left(\frac{\mathrm{d}C_{\mathrm{int}}}{\mathrm{d}t}\right)_{r_{\mathrm{f}},z}=\left(1/\left(1+\frac{D_{\mathrm{S}}}{D_{\mathrm{G}}}\frac{\Delta r}{\Delta r_{\mathrm{s}}}\frac{\Delta z}{h_{\mathrm{f}}}\frac{Kq_{\mathrm{m}}}{\left(1+KC_{\mathrm{int},z}\right)^2}\right)\right)\left(\left(\frac{\mathrm{d}C_{1,z}}{\mathrm{d}t}\right)_{r_{\mathrm{f}}+\Delta r/2,z}+\frac{D_{\mathrm{S}}}{D_{\mathrm{G}}}\frac{\Delta r}{\Delta r_{\mathrm{s}}}\left(\frac{\mathrm{d}q_{nr,z}}{\mathrm{d}t}\right)_{r_{\mathrm{f}}-\Delta r_s/2,z}\right) \quad (19)$$

$\left(\frac{\mathrm{d}C_{1,z}}{\mathrm{d}t}\right)_{r_{\mathrm{f}}+\Delta r/2,z}$ and $\left(\frac{\mathrm{d}q_{nr,z}}{\mathrm{d}t}\right)_{r_{\mathrm{f}}-\Delta r_s/2,z}$ are first calculated from Eqs. 14 and 12 and then $\left(\frac{\mathrm{d}C_{\mathrm{int}}}{\mathrm{d}t}\right)_{r_{\mathrm{f}},z}$ from Eq. 19.

Inside the adsorptive phase at $r_{\mathrm{s}}=0$, the boundary condition is:

$$\left(\frac{\mathrm{d}q}{\mathrm{d}r}\right)_{r_{\mathrm{s}},z}=0\quad\text{in}\,r_s=0 \quad (20)$$

Initial conditions:$t=0$, $C_{r,z}=C_{\mathrm{o}}$, $C_{1,z}=0$, $q_z=0$ for the equilibrium model, $C_{\mathrm{int},z}=0$ $q_{\mathrm{rs},z}=0$ for the solid diffusion model with C_{o} the initial VOC concentration in the gas sampler.Partial differential equations (Eqs. 5bis, 10bis, 11, 12, 14) are transformed by substituting finite-difference approximations. The alternating-direction implicit scheme provides a mean for solving parabolic equations in two spatial dimensions using tridiagonal matrices [27]. The tridiagonal system is solved by LU decomposition in two steps. A personal computer program is implemented in Fortran 90 language to simulate the concentration distribution in the gas sampler as a function of time.

Experimental

Reagents and materials

Studied VOCs are methyl vinyl ketone (MVK), supplied by Sigma-Aldrich (Steinheim, Germany), methyl methacrylate (MM), α-pinene and *n*-decane, supplied by Acros Organics (New Jersey, USA). All these reagents are at least 99% purity, except α-pinene (98%).

Standard gas generating device

Detailed principle of gas generation is described in previous papers [28, 29]. The device used here was designed and supplied by Calibrage (Saint Chamas, France). Briefly, single-compound atmospheres are generated by continuous injection of known amount of liquid VOC with a syringe pump (Harvard Apparatus, Les Ulis, France) into a measured and controlled airflow. Successive dry air (relative humidity less than 4% and temperature of 23°C) dilutions of concentrated gas are then applied to reach the desired concentrations.

Sampling devices

Two kinds of samplers are used: a Field Laboratory Emission Cell (FLEC®) described in the standard ISO 16000-10 [8] and especially modified for static SPME sampling [12] and a home-made cylindrical glass sampler (Fig. 3).

The FLEC® is made of acid-proof stainless steel, especially hand-polished to minimize sink effects. To avoid VOCs adsorption on the O-ring, the cell is equipped with a Viton® fluoroelastomer O-ring covered with Teflon® (Dimatrap, Pau, France). Moreover, a septum in polytetrafluoroethylene-silicone is screwed on the device for SPME fiber introduction. Finally, stainless steel tubes and quarter-turn valves are added to sweep standard gas through the device. Including these changes, the total sampling volume is evaluated at 70±5 mL. To solve boundary conditions of the model (Eqs. 6 and 7), the knowledge of boundary size of the sampler is required and deduced from the 2D drawing of FLEC® device. By applying a polynomial regression on the boundary curve, one obtains (unit in mm):

$$
\begin{array}{lll}
0 \le r \le 2 & Z_r = 21.7 & r^2 = 1 \\
2r \le 5 & Z_r = 22.84 r^{-0.07} & r^2 = 0.962 \\
5r \le 11 & Z_r = 146.1 r^{-1.24} & r^2 = 0.997 \\
11r \le 75 & Z_r = 30.42 r^{-0.54} & r^2 = 0.993 \\
0 \le z \le 2.8 & R_z = 75 & r^2 = 1 \\
2.8z \le 9 & R_z = 26.88 z^{-0.52} & r^2 = 0.990 \\
9z \le 18 & R_z = 158.7 z^{-1.29} & r^2 = 0.993 \\
18z \le 1.7 & R_z = -0.292 z^2 + 1.31 z + 20.2 & r^2 = 0.912
\end{array}
$$

The home-made cylindrical glass sampler shown in Fig. 3 has a radius (R) of 36.5 mm and is 77 mm high (Z) for a total volume of 340±10 mL.

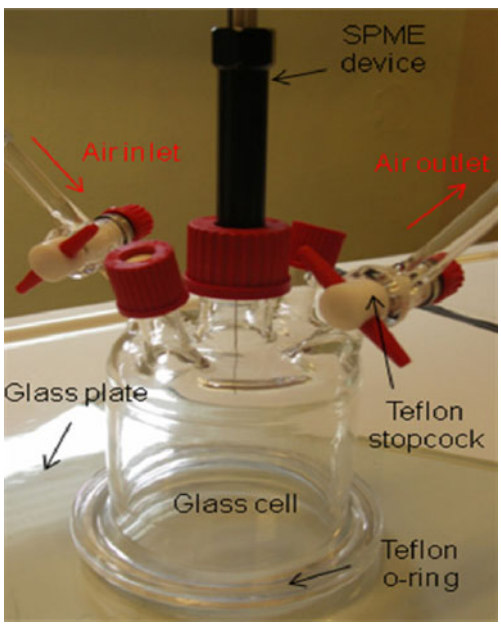

Fig. 3 Cylindrical sampler-SPME coupling systems

Sampling method

For material sampling, the emission cell (FLEC® or cylindrical sampler) is simply placed on the surface to be studied. Clean air is swept through the cell for 1 or 2 min at 1.4 $L min^{-1}$. To avoid over pressure in the cell, a by-pass system is added to the gas stream. The sampling chamber is then closed and the VOCs are allowed to diffuse from the material to the cell headspace until equilibrium state. Finally, the SPME fiber is introduced through the septum for VOCs extraction and determination of the gas phase concentration.

For calibration with standard gas, the emission cell (FLEC® or cylindrical sampler) is placed and tightened on a clean glass surface. From 1.6 to 3.2 L of standard gas is flushed through the system at 1.4 $L min^{-1}$. Then, the emission cell is closed to proceed to SPME extraction, under the same conditions than for materials. The cell is flushed by clean air between each experiment. For all trials, the temperature is regulated at 23±2°C.

Experimental isotherms of single compound are performed in 1 L cylindrical glass bulb equipped with Teflon stopcocks and a septum in the middle to introduce the SPME fiber according to previous works (1 extraction/glass bulb) [22].

Solid-phase microextraction

A manual SPME holder is used with a 75 μm PDMS-Carboxen fiber purchased from Supelco (Bellefonte, PA, USA). Fibers are conditioned in the GC injection port for 10 min at 300°C and at least 2 h at 300°C for new fibers. The extraction time varied from 1 to 30 min, the maximum allowed to limit the risk of contamination by the seal, which could adsorb/desorb VOCs.

Instrumentation

A Varian CP-3800 GC gas chromatograph (Varian, Les Ulis, France) equipped with an 1177 split/splitless injection port and a flame ionization detector (FID) is used for quantification analysis. The split/splitless injection port is equipped with a 0.75 mm i.d. liner, operated at 320°C. Carrier gas is helium with a flow rate of 2.0 mL min^{-1}. Chromatographic separations are performed using a VF-5 ms column (Varian, Les Ulis, France), 30 m×0.25 mm i.d., 0.25 μm film thickness, and the oven temperature is programmed as follows: 40°C for 4 min, then ramped at 15°C min^{-1} to 90°C (4 min) and finally ramped at 10°C min^{-1} to 250°C, held for 5 min. The temperature of the FID is 300°C. Signals are collected and treated with Varian Star Workstation software (Varian, Les Ulis, France).

Results and discussion

Adsorption kinetics depends on the physical properties of the adsorbent (specific surface area, pore size distribution, polarity, temperature) and physicochemical properties of the analyte (molecular structure and size, vapor pressure, dipolar moment, etc.). Microporous adsorbents are suitable for trapping small highly volatile organic molecules to allow capillary strength interaction between the adsorbate and the adsorbent. VOCs encountered in indoor air are indeed mainly small molecules requiring microporous material as Carboxen. In particular, this material based on activated carbon structure has a high affinity for apolar aromatic molecules. Another main parameter of the adsorption kinetics is the amount of analyte in the sampling device. That depends both on analyte concentration and on sampler volume. In SPME applications, the Carboxen coating is quite small, which limits its use for quantification of molecules due to the risk of competitive adsorption with other VOCs present in the sample. Therefore, coadsorption conditions should be deduced from the plots of kinetics defined as the quantity adsorbed on the fiber versus the exposure dose "$C_o.t$", where C_o is the VOC initial concentration and "t" the sampling time. Coadsorption range, corresponding to the calibration curve, is defined as linear part of kinetics where single and mixture VOCs are superimposed [12, 22].

Calibration curve modeling has been studied over the past 20 years [30]. In 1997, Ai proposed a theoretical model based on a diffusion-controlled mass transfer process to describe the entire kinetic process of SPME [31, 32]. In previous work, we proposed a model of adsorption kinetics for various volumes of cylindrical samplers in static sampling mode to estimate the calibration curve of toluene [33]. This model required the knowledge of both kinetic coefficients and the maximum adsorptive capacity. Its main advantage is that it can be solved analytically. However, it did not take into account the gas phase diffusion process, which is nevertheless a fundamental parameter of the mass transfer operation. To limit the number of unknown parameters (kinetics coefficients) and to include the gas phase diffusion, another approach, named equilibrium model, is considered here assuming that the gas phase diffusion is the rate-limiting step and that the adsorption process is reduced to equilibrium state. In addition, a model named solid diffusion model based on both the diffusion in gas and solid phases is also implemented to discuss the mechanism of mass transfer in the two kind of samplers studied.

Input data required for the equilibrium model are the Langmuir equation parameters (K, q_m), obtained from experimental isotherms of single compound, and the molecular diffusion coefficient in gas phase (D_G) estimated from the Fuller equation.

Determination of the input data of the equilibrium model

The experimental parameters of the Langmuir equation and the calculated gas phase diffusion coefficients are summarized in Table 1. The hyperbolic shape of the experimental isotherms is well defined by the Langmuir model. The values of the Langmuir constant K are in the same order level for the four VOCs studied: between 1.5×10^{-5} and 1.75×10^{-5} $m^3 nmol^{-1}$. This is explained by the superimposition of the equilibrium curves in the low concentration range. The high value of K, between 1.5×10^{-5} and 1.75×10^{-5} $m^3 nmol^{-1}$, showed the good affinity of the four compounds for the Carboxen, confirming that this fiber coating is convenient for the analysis of VOCs in indoor environments. The maximum adsorption capacity q_m is in the same order of magnitude, between 20 and 27 nmol, for MM, MVK and n-decane. However, the adsorption capacity for α-pinene is much lower with a value of 4 nmol. Due to the hyperbolic shape of the isotherms, the local equilibrium constant (dq/dC) of α-pinene is much lower than those of other compounds. This fact could be related to a weaker value of the adsorption enthalpy, representing weaker adsorbate–adsorbent interaction energy whatever the amount adsorbed. This could

Table 1 Input data of× the equilibrium model

Compound	Langmuir equation			Diffusion coefficient (Fuller)
	K (m^3 $nmol^{-1}$)	q_m (nmol)	r^2	D_G (m^2 s^{-1})
MVK	1.75×10^{-5}	22	0.963	9.16×10^{-6}
MM	1.75×10^{-5}	20	0.948	7.8×10^{-6}
α-pinene	1.5×10^{-5}	4	0.974	5.87×10^{-6}
Decane	1.75×10^{-5}	27	0.985	5.66×10^{-6}

be explained by the steric geometry of the molecule, a six-membered cyclic alkene with a four-membered ring above, which reduces the contact surface with the pore walls of the adsorbent.

Adsorption kinetics of four VOCs on SPME Carboxen fiber in cylindrical sampler

The experimental and modeled calibration curves of the four single VOCs on SPME Carboxen fiber in cylindrical sampler are plotted on the right side of Figs. 4, 5, 6, and 7. The equilibrium model for various initial concentrations C_o is tested and plotted on these figures. The main parameters of numerical model are summarized in Table 2. A good correlation is obtained between the equilibrium model and the experimental kinetics of MVK, MM and α-pinene in a large range of C_o t values. For n-decane, the model is in good agreement with experimental results in the linear part of the curve for C_o t values lower than 100 μmol m^{-3} min. For higher values, the results are slightly underestimated by the model.

The results of numerical calculation for a 1-h extraction time are shown in Table 3. This time is chosen to cover the range of experimental kinetics data. The numerical error ε and the extraction yield η of single VOC on the fiber are quantified by a VOC mass balance in the sampler at the beginning of the extraction and after 1 h. The stability of the numerical scheme is demonstrated by the very low values of the numerical error ε, in an order of magnitude between 10^{-6} and 10^{-9}%. C_{max} data is the maximum value of VOC concentration in gaseous phase after 1 h extraction estimated by the model at a local node of the numerical scheme. This parameter is used to test the quality of the numerical calculation and detect any problems of oscillation or divergence. η C_{max} is the extraction yield calculated assuming that C_{max} is the average concentration in the gas sampler. The values of η and η C_{max} are in the same order level because 1 h is close to the equilibrium time in the cylindrical sampler.

Regarding the mechanism of mass transfer in the cylindrical sampler, the validity of the equilibrium model showed that the limiting step is the molecular diffusion of VOC in gas phase. These results are consistent with previous work [33]. The fast adsorption step could be explained by the good affinity of the VOCs for the Carboxen, as shown by the isotherm data. Moreover, the thin adsorbent layer is an advantage in terms of adsorption site accessibility. Finally, the sampling rate corresponding to the slope of the calibration curve is much higher in the cylindrical sampler than in the FLEC® device (right side of Figs. 4, 5, 6, and 7). This sampling rate, or the total mass flux entering into the porous structure of the Carboxen fiber in steady-state regime for low values of C_o t, is a major parameter in the mechanism of intraparticle mass transfer in fibrous adsorbent. High sampling rate value is favorable to fast adsorption kinetics making valid the equilibrium model. This point will be further developed in the next section on the adsorption kinetics in FLEC® device.

Adsorption kinetics of four VOCs on SPME Carboxen fiber in FLEC® sampler

The experimental and modeled calibration curves of four single VOCs on SPME Carboxen fiber in the FLEC® are plotted on the left side of Figs. 4, 5, 6, and 7. The

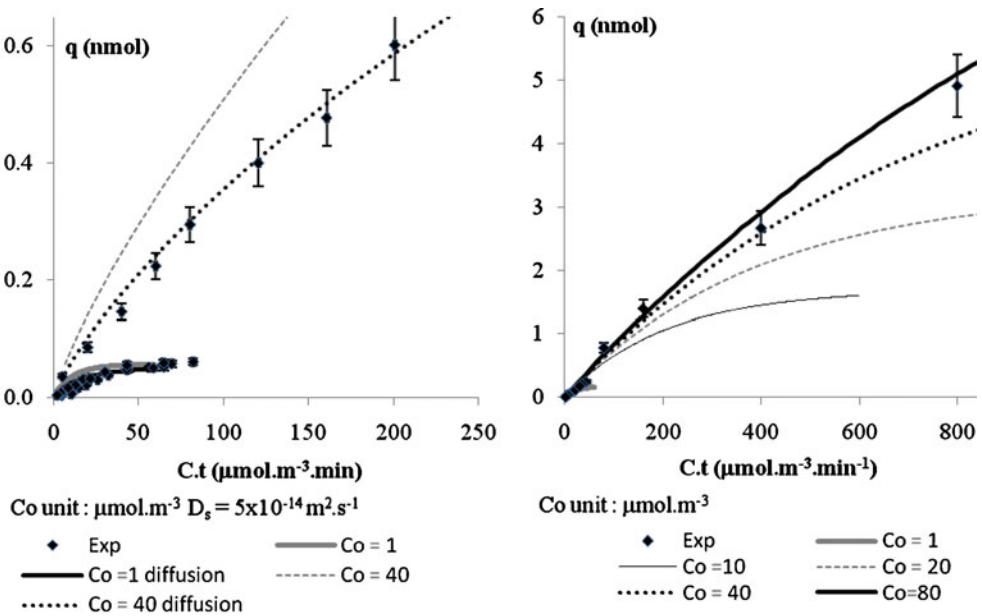

Fig. 4 Adsorption kinetics of MVK on SPME Carboxen fiber for various initial concentrations C_o in FLEC® (*left*) and cylindrical (*right*) samplers

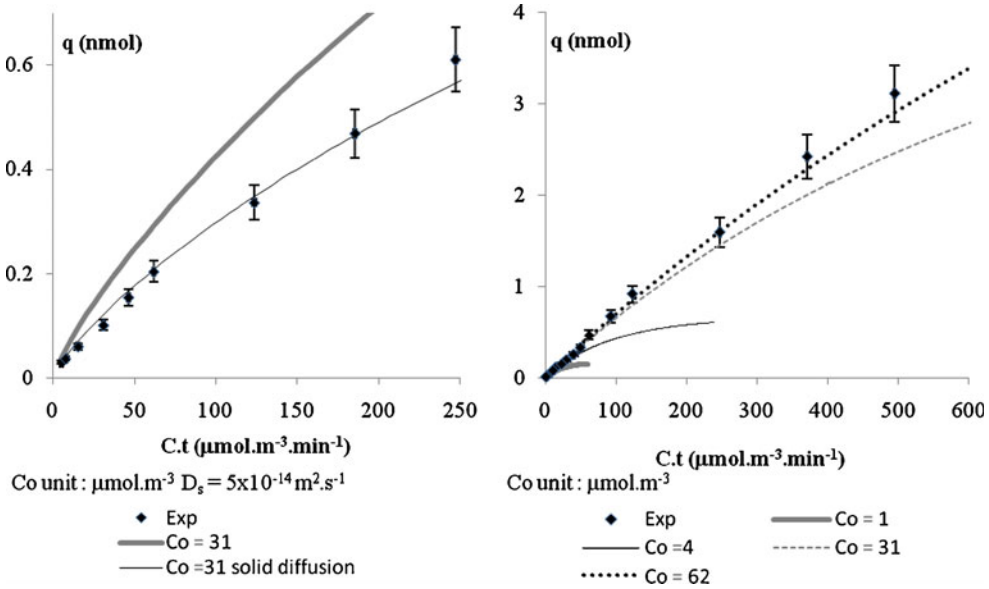

Fig. 5 Adsorption kinetics of MM on SPME Carboxen fiber for various initial concentrations C_o in FLEC® (*left*) and cylindrical (*right*) samplers

equilibrium and solid diffusion models for various concentrations C_o are tested and plotted on these figures. The discretization parameters of the solid diffusion model are summarized in Table 2. Figures 4, 5, 6, and 7 showed the invalidity of the equilibrium model for the FLEC® sampler as the calibration curves are overestimated. Therefore, contrary to the cylindrical sampler, the limiting step of mass transfer is not the gas phase but the solid phase of the Carboxen fiber. So, the solid diffusion model is convenient to fit experimental data. In this model, the solid diffusion coefficient D_S is considered as an adjustment parameter as it could not be estimated from the literature. These data are summarized in Table 4.

To investigate the mass transfer mechanism inside the fiber, the net diffusion coefficient D and the effective diffusivity D_e in porous media are calculated for each compound from Eqs. 24 and 25 presented in the Appendix section. For this purpose, sampling rate values in FLEC® and cylindrical devices are also quantified from the slope of the linear part of experimental adsorption kinetics and reported in Table 4. This sampling rate, or the total mass flux entering the porous structure of the Carboxen fiber in steady-state regime for low C_o t values, is mainly the sum of fluxes due to gaseous diffusion (molecular and/or Knudsen diffusion, depending on the pore radii) and surface diffusion. In pores of diameter greater than the mean free path of a molecule, diffusion occurs by a process of molecular diffusion but, if the molecular free path is much greater than the pore diameter, diffusion occurs by molecules colliding with the pore walls

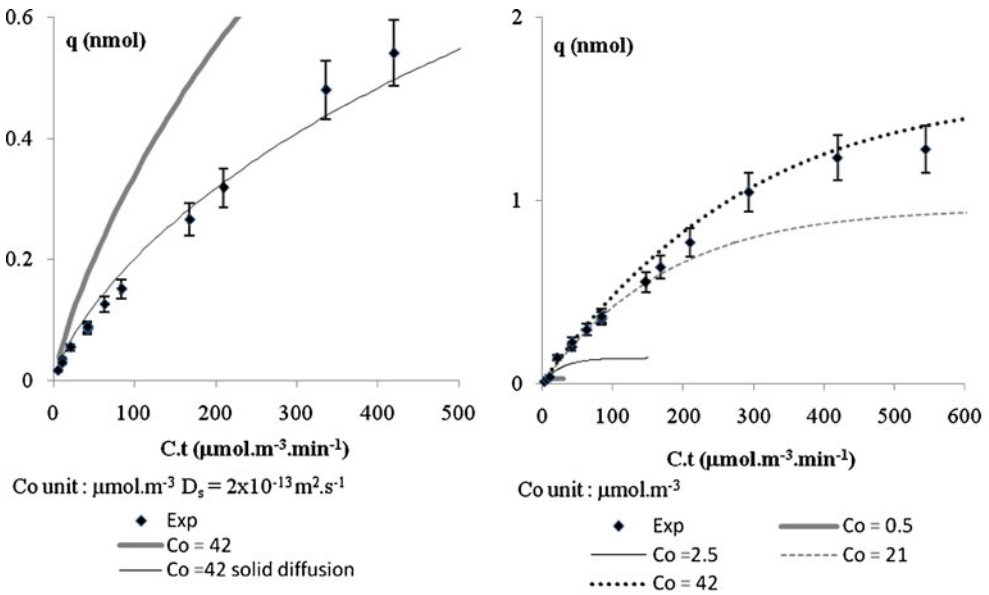

Fig. 6 Adsorption kinetics of α-pinene on SPME Carboxen fiber for various initial concentrations C_o in FLEC® (*left*) and cylindrical (*right*) samplers

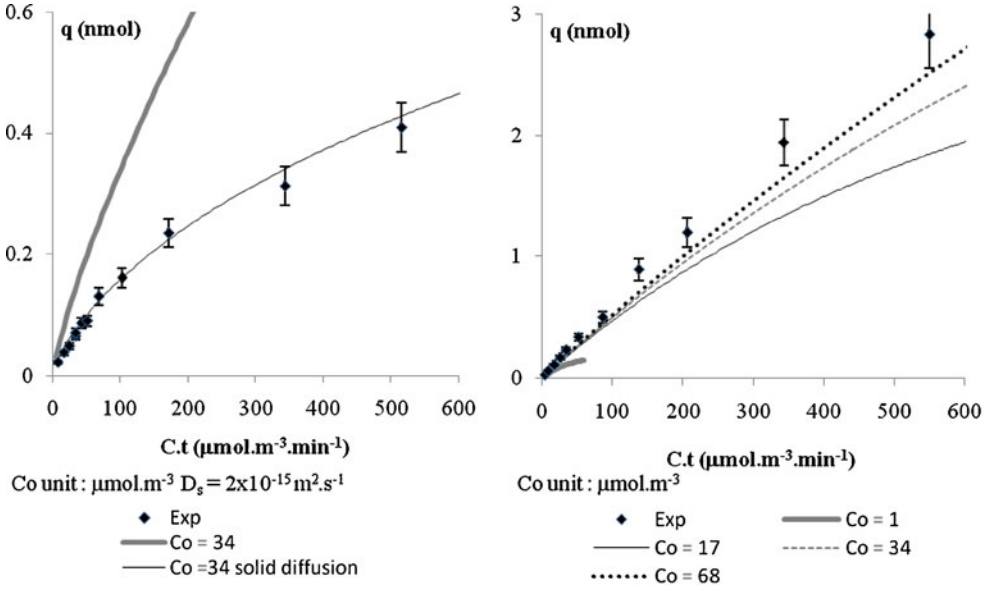

Fig. 7 Adsorption kinetics of decane on SPME Carboxen fiber for various initial concentrations C_o in FLEC® (*left*) and cylindrical (*right*) samplers

(Knudsen diffusion). The surface diffusion assumption is considered when molecules are transported across a surface rather than through the gaseous phase [34]. Consequently, surface diffusion occurred essentially in small size pores (micropores). It implies that a low adsorbate mass flux enters the pore to limit the gaseous diffusion, associated to strong adsorbate–adsorbent interaction energy to promote the adsorption of molecules at the pore surface rather than their diffusion inside the pore. The effect of gaseous diffusion on the intraparticle mass transfer is estimated by calculating the net diffusion coefficient D and the effective diffusivity D_e. The results in Table 4 showed high D and D_e values compared to the experimental D_S. This observation allows deducing the implicit assumption that the surface diffusion is the limiting step of the intraparticle mass transfer. This result is in agreement with previous work concerning VOCs adsorption on activated carbon fibers [35]. Moreover, the lowest values of sampling rates in the FLEC® compared to those in the cylindrical sampler are favorable to surface diffusion rather than gaseous diffusion. Finally, the good affinity of the studied VOCs for the Carboxen fiber is another advantage for the surface diffusion because of the quite strong adsorbate–adsorbent interaction energy. The greatest value of D_S for α-pinene (2×10^{-13} m^2s^{-1}), is consistent with its adsorbate–adsorbent interaction energy which is the lowest of studied compounds.

Analytical considerations

All the kinetics (Figs. 4, 5, 6 and 7) presents a linear part which is used for quantitative analysis. For the cylindrical sampler, the smallest linearity range is obtained for α-pinene (up to 300 µmol m^{-3} min) and the largest for MVK (up to 1200 µmol m^{-3} min). Thus, it is possible to quantify high emission concentrations (about 10 mg m^{-3}) by applying short extraction times (5 or 10 min). On the opposite, it is possible to detect µg m^{-3} level for longer extraction times, for example 30 min. Obviously, the FLEC® led to lower sensitivities as it is shown in Table 4: the sampling rates (slopes of the linear part of the kinetics) are two or three times lower than those obtained for the cylinder. The linearity ranges are also narrower: up to 40 µmol m^{-3} min for α-pinene and up to 200 µmol m^{-3} min for MVK. However, these calibration curves should be compared to those obtained with the same compound in mixture to define precisely the calibration range of each compound.

Table 2 Parameters of numerical simulation on cylindrical and FLEC® sampler

Cylindrical sampler		Discretization parameters				
Radius (m)	Height (m)	Δr (m)	Δz (m)	Δt (s)	Radial nodes	Axial nodes
3.65×10^{-2}	7.7×10^{-2}	10^{-4}	10^{-4}	10^{-3}	365	770
FLEC® device		Discretization parameters				
Radius	Height	Δr (m)	Δz (m)	Δr_s (m)	Radial fiber nodes	Δt (s)
See "Reagents and materials"		10^{-4}	10^{-4}	5×10^{-8}	1000	10^{-3}

Table 3 Results of numerical simulation of equilibrium model in cylindrical sampler: initial concentration (C_o), local maximum concentration of VOC in gas sampler (C_{max}) after 1 h extraction calculated by the equilibrium model, extraction yield calculated with C_{max} (η C_{max}), extraction yield (η), numerical error (ε)

Compound	C_o (μmol m^{-3})	C_{max} (μmol m^{-3})	η C_{max} (%)	η (%)	ε(%)
MVK	1	0.496	50.4	50.66	7.8×10^{-8}
	10	5.078	49.22	49.47	8.5×10^{-7}
	20	10.425	47.87	48.08	1.7×10^{-6}
	40	22.002	45.00	45.14	3.4×10^{-6}
	80	48.908	38.86	38.90	6.7×10^{-6}
MM	1	0.531	46.90	47.28	2.0×10^{-9}
	4	2.138	46.55	46.92	2.9×10^{-7}
	31	17.637	43.11	43.35	2.3×10^{-6}
	62	38.012	38.69	38.80	4.7×10^{-6}
Decane	1	0.541	45.90	49.79	4.5×10^{-8}
	17	9.346	45.02	45.88	7.6×10^{-7}
	34	19.028	44.03	44.81	1.5×10^{-6}
	68	39.624	41.73	42.33	3.1×10^{-6}
α-pinene	0.5	0.412	17.60	17.61	7.0×10^{-8}
	2.5	2.069	17.22	17.22	2.6×10^{-7}
	21	18.032	14.13	14.13	2.0×10^{-6}
	42	37.125	11.6	11.6	3.7×10^{-6}

Conclusions

Static sampling is recently studied for the measurement of VOCs emission from materials in indoor environments. One method consists in coupling existing (e.g., FLEC®) or home-made emission devices with SPME pre-concentration. To simplify the calibration procedure, which is not easy to implement, modeling approaches can be considered. In this paper, an equilibrium model based on Langmuir isotherm for prediction of adsorption kinetics (i.e., calibration curves) of single VOC in a home-made cylindrical emission cell is proposed. Results showed good correlation between experimental and calculated data, assessing the relevance of this approach. However, this model is not suitable for low volume samplers like the FLEC®. The sampling rate, depending on the sampler volume, influenced the intraparticle mass transfer. High values of sampling rate are favorable to fast adsorption kinetics making valid the equilibrium model. In this case, the limiting step of mass transfer is the molecular diffusion of VOC in gas phase. In the FLEC® cell, due to low volume implying low sampling rate, the limiting step is the mass transfer inside the fiber. That required to use the solid diffusion model and surface diffusion is identified as the limiting step of the intraparticle mass transfer. This model is less convenient to use because it required the knowledge of the solid diffusion coefficient D_S, which is an unknown parameter.

In fact, the amount of VOC available in gas phase, depending on the sampler volume, had an essential influence on the gas/fiber mass transfer mode. Thus, this parameter governs the sampling rate of VOC on Carboxen SPME fiber.

In summary, the equilibrium model is an interesting tool to estimate calibration curves of VOCs for samplers of volume greater than or equal to 340 mL in the aim of quantification of building material emission. For samplers of low volumes like FLEC® device, the model based on intraparticle mass transfer, which involves the surface diffusion, is appropriate. Regarding analytical consider-

Table 4 Results of numerical simulation of solid diffusion model in FLEC® sampler and comparison with cylindrical sampler: net diffusion coefficient (D), effective diffusivity (D_e), solid diffusion coefficient (D_S), initial concentration (C_o), extraction yield (η), numerical error (ε) after 1 h extraction calculated by the solid diffusion model, sampling rate in FLEC and cylindrical sampler

VOC	D	D_e	D_S	C_o	η	ε	Sampling rate mL min^{-1}	
	m^2 s^{-1}	m^2 s^{-1}	m^2 s^{-1}		%	%	FLEC	Cylinder
MVK	1.65×10^{-7}	6.60×10^{-8}	5×10^{-14}	40	71	4.2×10^{-9}	3.5	6.9
MM	1.39×10^{-7}	5.54×10^{-8}	5×10^{-14}	31	69	3.1×10^{-9}	3.4	7.5
α-Pinene	1.13×10^{-7}	4.74×10^{-8}	2×10^{-13}	42	37	3.1×10^{-8}	2.0	5.5
Decane	1.16×10^{-7}	4.64×10^{-8}	2×10^{-15}	34	36	1.4×10^{-8}	1.85	5.8

ation, better performances in terms of sensitivity and linearity are also determined for the sampler having the highest volume (cylinder). Moreover, it is also cost effective and will be considered for further works for on-site multipoint sampling.

Appendix

Abbreviations

C	Gas concentration of compound in the element (=$C_{r,z}$; nmol m^{-3})
C_{max}	Modeled local maximum concentration of VOC in gas sampler after 1 h extraction
C_o	Initial concentration of VOC in gas sampler before extraction step (nmol m^{-3})
$C_{r,z}$	Concentration of compound in the element in coordinates r,z (nmol m^{-3})
$C_{1,z}$	Concentration in the element in contact with the fiber in coordinate z (nmol m^{-3})
$C_{int,z}$	Concentration at the gas/fiber interface in coordinates r_f, z (nmol m^{-3})
D	Net diffusion coefficient of the compound inside the fiber (m^2 s^{-1})
D_e	Effective diffusivity in the fiber (m^2 s^{-1})
D_G	Molecular diffusion coefficient of compound in gas phase (m^2 s^{-1})
D_K	Knudsen diffusion in micropores (m^2 s^{-1})
D_s	Diffusion coefficient of compound inside the fiber (m^2 s^{-1})
F_{ai}	Axial diffusive flow entering the element (nmol s^{-1})
F_{ao}	Axial diffusive flow leaving the element (nmol s^{-1})
F_{ri}	Radial diffusive flow entering the element (nmol s^{-1})
F_{ro}	Radial diffusive flow leaving the element (nmol s^{-1})
h_f	Height of the fiber (m)
K	Langmuir constant (m^3 nmol^{-1})
M_A	Molecular weight of the compound (g mol^{-1})
M_B	Molecular weight of air=28.8 (g mol^{-1})
P	Total pressure (bar)
q_z	Amount adsorbed of compound on the fiber in axial coordinate z (nmol)
$q_{int,z}$	Amount adsorbed at the gas/fiber interface in coordinates r_f, z (nmol)
q_m	Maximum amount adsorbed (nmol)
$q_{nr,z}$	Amount adsorbed in the external element of the fiber in contact with gas phase in axial coordinate z (nmol)
$q_{rs,z}$	Amount adsorbed in an element inside the fiber in coordinates r_s, z (nmol)
r	Radial coordinate in the sampler (gas phase; m)
r_f	Radius of the fiber (m)
r_p	Mean radius of pores (m)
r_s	Radial coordinate inside the fiber (m)
t	Time (s)
T	Temperature (°K)
$V_{r,z}$	Volume of the element located in coordinates r,z (=$2\pi r\Delta r\Delta z$)
z	Axial coordinate in the gas sampler and the fiber (m)
ε	Numerical error of simulation after 1 h extraction (deduced by comparing mass balance in the gas sampler and fiber at the beginning and the end of simulation)
ε_p	Fiber porosity
η	SPME extraction yield (%)
$\eta_{C_{max}}$	SPME extraction yield calculated with C_{max} (%)
ν	Atomic diffusion volume increment
τ	Pore tortuosity factor
Δr	Radial thickness of the element in gas phase (m)
Δz	Axial thickness of the element in gas phase (m)
Δr_s	Radial thickness of the element inside the fiber (m)

Estimation of diffusion coefficients in gas phase and adsorptive phase

The molecular diffusion coefficient in gas phase D_G is calculated from the following equation [25]:

$$D_G = \frac{0.001437^{1.75}}{PM_{AB}^{1/2}\left[\left(\sum V\right)_A^{1/s}+\left(\sum V\right)_B^{1/s}\right]^2} \quad (21)$$

where

$$M_{AB} = \frac{2}{\left(\frac{1}{M_A}+\frac{1}{M_B}\right)} \quad (22)$$

M_A and M_B are the molecular weights of single VOC and air, ν the atomic diffusion volume increment, P the total pressure and T the temperature.

In pores of diameter much greater than the mean free path of a molecule, diffusion occurs by a process of molecular diffusion but, if the molecular free path is much greater than the pore diameter, diffusion occurs by molecules colliding with the pore walls (Knudsen diffusion).

The Knudsen diffusion D_K is deduced from the equation below [36]:

$$D_K = 9700 r_p \left(\frac{T}{M_A}\right)^{1/2} \quad (23)$$

with r_p the mean radius of pores.

When the mean free path and pore radius are of similar magnitude, the net diffusion coefficient D is calculated in

proportion to the individual molecular and Knudsen diffusivities. The net diffusion coefficient [34] is given by

$$D = \left(\frac{1}{D_G} + \frac{1}{D_K}\right)^{-1} \quad (24)$$

But diffusing molecules have to travel longer distances than if the pores are straight then the effective diffusivity D_e can be estimated from the following equation [34]:

$$D_e = \frac{s_p D}{\tau} \quad (25)$$

with ε_p the Carboxen porosity, τ the pore tortuosity factor.

The tortuosity factor τ can be approached by the equation below [36]:

$$\tau = \varepsilon_p + 1.5(1 - \varepsilon_p) \quad (26)$$

The effective diffusivity D_e is compared to the solid diffusion coefficient D_S deduced from the theoretical model to discuss the intraparticle transport resistances.

References

1. Le Cloirec P (ed) (1998) Les composés organiques volatils dans l'environnement. Lavoisier, Paris
2. Alsmo T, Holmberg S (2007) Indoor Built Environ 16:548–555
3. Chai M, Pawliszyn J (1995) Environ Sci Technol 29:693–701
4. ECA (1997) Indoor Air Quality & Its Impact On Man, Report 18, Evaluation of VOC emissions from building materials, Luxembourg, Office for Official Publications of the European Communities
5. AgBB (2008) Health-related evaluation procedure for volatile organic compounds emissions (VOC and SVOC) from building products
6. AFSSET (2009) Procédure de qualification des produits de construction et de décoration sur la base de leurs émissions de COV et de formaldéhyde et de critères sanitaires, Rapport du groupe de travail Afsset «COV et produits de construction», saisine 2004/011. Agence Française de Sécurité Sanitaire de l'Environnement et du Travail (AFSSET), Paris
7. International Organization for Standardization (ISO)—ISO 16000-9 (2006) Indoor Air. Part 9: determination of the emission of volatile organic compounds from building products and furnishing-Emission test chamber method
8. International Organization for Standardization (ISO)—ISO 16000-10 (2006) Indoor Air. Part 10: determination of the emission of volatile organic compounds from building products and furnishing-Emission test cell method
9. Shinohara N, Fujii M, Yamasaki A, Yanagisawa Y (2007) Atmos Environ 41:4018–4028
10. Shinohara N, Kai Y, Mizukoshi A, Fujii M, Kumagai K, Okuizumi Y, Jona M, Yanagisawa Y (2008) Build Environ 44:859–863
11. Blondel A, Plaisance H (2010) Analytical methods 2(12):2032–2038
12. Nicolle J, Desauziers V, Mocho P (2008) J Chromatography A 1208:10–15
13. Nicolle J, Desauziers V, Mocho P, Ramalho O (2009) Talanta 80:730–737
14. Koziel J, Jia M, Pawliszyn J (2000) Anal Chem 72:5178–5186
15. Tuduri L, Desauziers V, Fanlo JL (2001) J Chromatogr Sci 39:521–529
16. Tuduri L, Desauziers V, Fanlo JL (2003) Analyst 128:1028–1032
17. Gorecki T, Pawliszyn J (1997) Analyst 124:1079–1086
18. Bouvier-Brown NC, Holzinger R, Palitzsch K, Goldstein AH (2007) J Chromatogr A 1161(1–2):113–120
19. Ferrari F, Sanusi A, Millet M, Montury M (2004) Anal Bioanal Chem 379(3):476–483
20. Chen Y, Koziel JA, Pawliszyn J (2003) Anal Chem 75(23):6485–6493
21. Paschke A, Vrana B, Popp P, Schürmann G (2006) Environ Pollut 144(2):414–422
22. Larroque V, Desauziers V, Mocho P (2006) J Environ Monit 8:106–111
23. Lestremau F, Anderson FAT, Desauziers V, Fanlo JL (2003) Anal Chem 75:2626–2632
24. Larroque V, Desauziers V, Mocho P (2006) Anal Bioanal Chem 386:1457–1464
25. Fuller EN, Schettler PD, Giddings JC (1966) Ind Eng Chem 58 (5):18–27
26. Langmuir L (1918) J Am Chem Soc 40:1361–1366
27. Chapra SC, Canale RP (eds) (1988) Numerical methods for engineers, 2nd edn. McGraw-Hill, New York
28. Desauziers V (2004) Trends Anal Chem 23:252–260
29. Koziel J, Martos PA, Pawliszyn J (2004) J Chromatograph A 1025:3–10
30. Ouyang G, Pawliszyn J (2008) Anal Chim Acta 627:184–197
31. Ai J (1997) Anal Chem 69:1230–1236
32. Ai J (1997) Anal Chem 69:3260–3266
33. Mocho P, Larroque V, Desauziers V (2007) Anal Bioanal Chem 388:147–156
34. Crittenden B, Thomas J (eds) (1998) Adsorption technology & design, 1st edn. Butterworth-Heinemann, Oxford
35. Fournel L, Mocho P, Brown R, Le Cloirec P (2010) Adsorption 16 (3):147–153
36. Tien C (ed) (1994) Adsorption calculations and modeling. Butterworth-Heinemann, Boston